ORIGINAL ARTICLE
(CC BY-SA)
UDC: 616.718.5-001.5-089
DOI: https://doi.org/10.2298/VSP260305030Y

Early diagnosis and optimization of intraoperative management strategies for posterior tibial tendon entrapment following ankle fractures in the elderly

Rana dijagnoza i optimizacija intraoperativnih strategija lečenja za uklještenje zadnje tibijalne tetive nakon preloma skočnog zgloba kod starijih osoba

Shuo Yang*†, Yang Lu*, Jiliang Jiang*

***Jiangsu Province Hospital on Integration of Chinese and Western Medicine, Department of Orthopedics, Nanjing, Jiangsu, China; †Tongji University School of Medicine, Shanghai, China**

Abstract

Background/Aim. Posterior tibial tendon (PTT) entrapment is a rare, often underdiagnosed, but severe complication of complex ankle fractures. The aim of the study was to determine the characteristics of PTT entrapment in elderly patients with ankle fractures, and to establish a predictive model based on preoperative available clinical and imaging data. **Methods.** The study enrolled a total of 130 elderly patients treated between 2019 and 2024. Data were retrospectively analyzed, and all patients completed a minimum follow-up period of 12 months. Using intraoperative confirmation as the gold standard, a basic clinical logistic regression (LR) model was compared with an imaging-enhanced LR model (incorporating fracture fragment count and PTT sheath involvement), a random forest (RF) model, and a support vector machine (SVM). Performance was validated *via* 5-fold cross-validation, area under the receiver operating characteristic (ROC) curve (AUC), calibration, and decision curve analysis (DCA). **Results.** PTT entrapment occurred in 29.2% (38/130) of patients, primarily located in the posterior fracture gap (68.4%) or medial malleolus (31.6%). Morphological findings included simple mechanical incarceration (50.0%), soft tissue adhesion (36.8%), and tendon surface injury (13.1%). The imaging-enhanced LR model significantly outperformed the basic model (AUC 0.89 vs. 0.72) and exceeded RF (0.85) and SVM (0.88) models. DCA demonstrated high net benefit across risk levels, and intraoperative findings showed high consistency with imaging-based predictions. **Conclusion.** PTT entrapment is common in elderly ankle fractures. An imaging-enhanced predictive model based on preoperative computed tomography fracture morphology and local anatomy enables effective risk assessment, providing a reliable reference for targeted intraoperative exploration and surgical management strategies.

Keywords:
aged; ankle fractures; diagnosis; models, statistical; prognosis; tendon entrapment.

Apstrakt

Uvod/Cilj. Uklještenje zadnje tibijalne tetive (*posterior tibial tendon* – PTT) predstavlja retku, često nedovoljno prepoznatu, ali ozbiljnu komplikaciju složenih preloma skočnog zgloba. Cilj rada bio je da se utvrde karakteristike uklještenja PTT kod starijih pacijenata sa prelomima skočnog zgloba i da se uspostavi prediktivni model zasnovan na preoperativno dostupnim kliničkim i podacima medicinskih snimanja. **Metode.** U studiju je bilo uključeno ukupno 130 starijih pacijenata lečenih u periodu između 2019. i 2024. godine. Podaci su retrospektivno analizirani, a svi pacijenti su praćeni u minimalno 12 meseci. Koristeći intraoperativnu potvrdu kao zlatni standard, osnovni model logističke regresije (LR) zasnovan na kliničkim podacima upoređen je sa LR modelom unapređenim podacima medicinskih snimanja (koji uključuje broj fragmenata preloma i zahvaćenost omotača PTT), modelom „slučajne šume“ (*random forest* – RF) i algoritmima *support vector machine* (SVM). Učinak je validiran pomoću petostruke unakrsne validacije, površine ispod krive *receiver operating characteristic* (ROC) – AUC, kalibracije i analize krive odlučivanja (*decision curve analysis* – DCA). **Rezultati.** Uklještenje PTT registrovano je kod 29,2% (38/130) pacijenata, primarno lokalizovano u zadnjem delu preloma (68,4%) ili u medijalnom maleolusu (31,6%). Morfološki nalazi uključivali su jednostavno mehaničko uklještenje (50,0%), adheziju mekog tkiva (36,8%) i oštećenje površine tetive (13,1%). Model LR unapređen podacima medicinskih snimanja značajno je nadmašio osnovni model (AUC 0,89 vs. 0,72) i premašio modele RF (0,85) i SVM (0,88). DCA je pokazala visoku neto korist kroz različite nivoe rizika, a

Correspondence to: Jiliang Jiang, Jiangsu Province Hospital on Integration of Chinese and Western Medicine, Department of Orthopedics, Nanjing 210 028, Jiangsu Province, China. E-mail: jiangjljphicwm@sdsch.cn

intraoperativni nalazi bili su u velikoj meri usklađeni sa predikcijama zasnovanim na medicinskim snimcima. **Zaključak.** Uklještenje PTT je česta pojava kod preloma skočnog zgloba kod starijih osoba. Prediktivni model unapređen podacima medicinskog snimanja, zasnovan na preoperativnoj morfologiji preloma dobijenoj kompjuterizovanom tomografijom i lokalnoj anatomiji, omogućava efikasnu procenu rizika, pružajući pouzdanu osnovu za ciljano intraoperativno istraživanje i strategije hirurškog lečenja.

Ključne reči:
stare osobe; skočni zglob, prelomi; dijagnoza; modeli, statistički; prognoza; tetiva, uklještenje.

Introduction

As the population continues to age rapidly, the incidence of ankle fractures (AFs) among the elderly is rising, making it one of the most common lower limb injuries in this age group [1]. Compared to younger patients, elderly individuals are more likely to present with osteoporosis, complex fracture patterns, and poor soft tissue conditions, all of which increase the difficulty of surgical management [2, 3]. Therefore, the treatment objective is not only to achieve stable reduction and internal fixation, but also to minimize the risk of missing critical structural injuries and preventing subsequent postoperative dysfunction [4, 5].

The posterior tibial tendon (PTT) is a key dynamic structure that maintains medial ankle stability and arch integrity and plays an important role in gait, weight-bearing transmission, and coordinated ankle movement [6]. In AFs, particularly those involving the posterior or medial malleolus, the normal course and gliding environment of PTT may be disrupted by displaced fragments, fragment incarceration, or altered anatomical relationships. This may result in entrapment, restricted mobility, or even damage to the tendon surface [7]. However, due to its deep anatomical location, PTT involvement often lacks specific clinical manifestations. Preoperative physical examination and routine imaging provide limited information, leading to frequent underestimation or oversight in clinical practice [8, 9]. Additionally, because of the difficulty in preoperative identification, PTT entrapment is often only recognized intraoperatively when reduction is impeded, or postoperatively when poor reduction, persistent pain, or functional limitations are observed. Missed or delayed diagnosis may require revision surgery and negatively affect recovery [10].

The previous study on PTT entrapment has mainly consisted of case reports or small retrospective series, focusing on intraoperative management rather than systematic risk assessment [11]. In elderly patients, osteoporosis and comminuted fractures further complicate fracture morphology, making abnormal tendon course or entrapment difficult to identify through routine imaging. Reliance on intraoperative exploration alone is, therefore, inherently passive and uncertain. Currently, quantitative studies assessing the risk of PTT entrapment based on preoperative clinical and imaging features are lacking. Moreover, existing studies are largely descriptive, and few have linked predictive findings with intraoperative morphology or surgical complexity, limiting their clinical applicability [12, 13]. Therefore, identifying high-risk patients preoperatively and optimizing intraoperative strategies remains an important but underexplored issue.

Based on this background, the present study systematically analyzed the characteristics of PTT entrapment in elderly patients with AFs and aimed to construct a predictive model using preoperative clinical and imaging data. In addition, intraoperative morphological observations were incorporated to explore the relationship between predictive results and surgical findings, providing a practical approach for preoperative risk assessment and intraoperative management.

Methods

Study design and subjects

This single-center retrospective cohort study consecutively enrolled 130 elderly patients who underwent open reduction and internal fixation for AFs at our hospital between December 2019 and December 2024. Based on intraoperative findings of PTT entrapment, patients were categorized into two groups: the entrapment group and the non-entrapment group. The study protocol was approved by the Ethics Committee of Jiangsu Province Hospital on Integration of Chinese and Western Medicine (from December 20, 2019). Informed consent was waived due to the retrospective study design.

Sample size estimation

Due to the retrospective design of this study, the sample size consisted of all eligible cases consecutively collected during the study period. The primary outcome was the presence or absence of intraoperative PTT entrapment. Following general principles for predictive modeling, the sample size of the logistic regression (LR) model should match the number of candidate predictor variables to ensure the robustness of model estimation. In this study, the number of independent variables was strictly controlled during modeling, and the regularized LR model was used to mitigate overfitting risk. Furthermore, model performance was internally validated using 5-fold cross-validation. Based on the above strategies, the sample size was deemed sufficient for predictive model construction and preliminary validation.

Inclusion and exclusion criteria

Inclusion criteria were as follows: patients aged ≥ 65 years; a diagnosis of isolated malleolar, bimalleolar, or trimalleolar fractures; completion of a preoperative ankle computed tomography (CT) examination; undergoing in-

traoperative exploration of PTT to confirm entrapment; and a postoperative follow-up period of ≥ 12 months.

Exclusion criteria were as follows: patients with a history of severe injury or prior surgery of the ipsilateral ankle joint; concurrent pathological fracture or infectious disease; severe neuromuscular system disease affecting lower limb function; or incomplete imaging or follow-up data.

Collection of baseline clinical variables

Demographic variables included age and sex. Body mass index (BMI) was calculated based on preoperative height and weight. The affected side was recorded. Fracture-related clinical characteristics included fracture type and extent of involvement. Fractures were classified as isolated malleolar, bimalleolar, or trimalleolar based on preoperative imaging assessment. Follow-up duration was defined as the time interval from the date of surgical completion to the last follow-up and was reported in months. Osteoporosis status was determined based on preoperative bone mineral density examination or previous diagnosis. Osteoporosis was defined as a T-value ≤ – 2.5 in patients who underwent dual-energy X-ray absorptiometry [14]. Patients who failed to obtain preoperative bone mineral density values were also classified as osteoporosis if the diagnosis of osteoporosis had been clearly documented in the previous medical record with corresponding treatment.

Collection of preoperative imaging variables

Preoperative imaging variables were derived from routine imaging examinations performed after admission and before surgery, including ankle X-ray and CT scans. All imaging assessments were performed preoperatively and excluded any intraoperative findings. Posterior malleolar fracture involvement was defined as involvement of the posterior tibial margin forming an independent fracture fragment. The number of fracture fragments was assessed. Two physicians experienced in foot and ankle surgery independently interpreted the images without knowledge of surgical outcomes and stratified the findings based on fragment number. For ease of model construction and analysis, stratification results were further classified into two categories, with fragment number ≥ 2 defined as multiple fragments and < 2 as fewer fragments [15]. A positive finding of PTT sheath involvement was defined *via* CT as a fracture line extending into the PTT sheath or a fracture fragment significantly altering the tendon's course, resulting in direct contact or compression.

Definition of outcome variables and intraoperative morphological verification

The outcome was the presence or absence of intraoperative PTT entrapment. During fracture reduction and fixation, an experienced foot and ankle surgeon directly examined PTT to confirm whether it was embedded within the fracture gap or constrained by soft tissue. PTT entrapment was defined as positive if the tendon was located within the fracture gap, formed mechanical incarceration with fracture fragments, or required release/traction to restore normal course. For patients who were confirmed to have PTT entrapment intraoperatively, the following morphological characteristics were further recorded: entrapment site (posterior AF gap, medial malleolus fragment space, etc.) and entrapment pattern (simple mechanical entrapment, concurrent soft tissue adhesion, concurrent tendon surface injury). The above intraoperative findings served as a morphological verification basis for imaging predictive results.

Construction of basic and imaging-enhanced logistic regression predictive models

To construct a control model for predicting the risk of PTT entrapment and avoid potential information leakage, a basic LR model without incorporating imaging enhancement features was first established based on preoperative baseline clinical and fracture morphology variables. Candidate independent variables included age, osteoporosis status, and posterior malleolar fracture involvement. Considering the sample size and event number limitations, L2 regularization was applied to reduce overfitting risk and enhance parameter estimation robustness.

Based on the basic model, preoperative imaging enhancement features, including fracture fragment number stratification and PTT sheath involvement, were further incorporated to construct an imaging-enhanced LR model, used to evaluate the incremental value of imaging structure information for the predictive performance of the model.

To ensure robustness of model performance, all LR models underwent internal validation using 5-fold stratified cross-validation. Within each fold, the model was fitted on the training set and generated predicted probabilities on the corresponding validation set for subsequent discriminatory power, calibration performance, and decision curve analysis (DCA).

Construction of a machine learning predictive model

To verify the predictive consistency of imaging enhancement features across different modeling strategies and serve as performance control, random forest (RF) and support vector machine (SVM) models were further constructed using the same set of preoperative clinical and imaging variables. Given the relatively limited sample size, this study did not employ complex nested cross-validation or large-scale parameter search. Instead, models were constructed using preset conventional parameter settings to reduce the risk of overfitting and enhance model reproducibility. The RF model used a fixed number of decision trees and limited the maximum depth of a single tree. The SVM model used a radial basis function kernel and default penalty parameters. Consistent with the LR models, RF and SVM models also underwent internal validation using 5-fold stratified cross-validation. The predict-

ed probabilities generated by each model during cross-validation were used for uniform performance evaluation and comparison.

Evaluation of discriminatory power and classification performance of predictive models

The discriminatory power of models was assessed using receiver operating characteristic (ROC) curves, with area under the curve (AUC) as the primary metric for the capability of the model to distinguish patients with and without PTT entrapment. With the predicted probability threshold uniformly set at 0.5, the sensitivity, specificity, and overall accuracy of each model were calculated.

Calibration performance evaluation

For the final selected imaging-enhanced LR model, its calibration performance for predicted probability was evaluated. Calibration performance measured the consistency between the model's predicted probability of PTT entrapment occurrence and the actual incidence rate. The model's predicted probabilities were grouped by magnitude, and the mean predicted probability and corresponding actual incidence rate were calculated for each group. They were graphically compared against the ideal calibration curve to visually illustrate the model's calibration across different risk intervals. Meanwhile, the Brier score was employed to quantitatively assess the model's overall calibration performance. The Brier score was defined as the mean of the squared differences between predicted probabilities and actual outcomes.

Decision curve analysis

To assess the potential value of the imaging-enhanced LR model in clinical decision-making, the model was further evaluated using DCA. Using DCA, the clinical utility of the imaging-enhanced LR model was assessed by comparing the net benefit of different decision strategies across a range of threshold probabilities. The threshold probability represented the clinical risk threshold for further intraoperative exploration or intervention. When the predicted probability was higher than this threshold, intervention was considered justified. Net benefit calculation comprehensively considered both true positive and false positive results and was defined as the trade-off between the benefit of correctly identifying events and the cost of unnecessary interventions at a given threshold probability.

Interpretability analysis

To elucidate the predictive contribution of each variable in the imaging-enhanced LR model, standardized regression coefficients and their corresponding odds ratios (OR) were examined. Continuous variables were normalized prior to model fitting to ensure comparability of coefficients. Regression coefficients and OR were used to assess the direction, magnitude, and strength of association between predictors and the outcome.

Risk stratification and intraoperative grading processing algorithms

Based on the predicted probabilities generated by the imaging-enhanced LR model, subjects underwent preoperative risk stratification. Patients were categorized into low-, medium-, and high-risk groups according to preset probability thresholds, reflecting their relative risk of PTT entrapment. This risk stratification was conducted based solely on preoperative information and did not incorporate any intraoperative findings. Based on preoperative risk stratification, an intraoperative grading algorithm was constructed by considering direct observation of the PTT status intraoperatively. Intraoperative grading was completed mainly based on the presence or absence of PTT entrapment, its severity, and the integrity of the tendon and surrounding soft tissue. The entrapment was divided into grades 0–3. Grade 0 (no entrapment): no PTT entering the fracture gap was found intraoperatively, and the tendon ran naturally without obvious traction or obstruction. Grade 1 (mild and reversible entrapment): PTT was partially embedded in the fracture gap or obscured by soft tissue, but without obvious adhesion. After mild traction or partial release, it could be successfully reduced without structural damage. Grade 2 (deep entrapment with soft tissue adhesion): PTT was deeply embedded in the fracture gap of the posterior ankle or medial ankle, often accompanied by obvious soft tissue adhesion, and it was difficult to release the entrapment by simple traction. Grade 3 (entrapment + tendon injury): abrasions, partial tear, or structural integrity of the PTT surface was visible during the process of release. Grading assessment was performed by the surgeon during fracture reduction and fixation and was used to standardize intraoperative assessment and treatment procedures. Through this approach, the results of preoperative risk stratification were linked with the intraoperative grading process to explore the feasibility of preoperative assessment based on predictive models in guiding intraoperative decision-making.

Statistical analysis

Statistical analysis was performed using Python 3.11 software, primarily relying on statistical and machine learning analysis libraries such as SciPy and scikit-learn. The *t*-test was used for intergroup comparisons regarding continuous variables. Categorical variables were analyzed using the Chi-square test. The level of statistical significance was defined for $p < 0.05$.

Results

Baseline data

This study included 130 elderly patients with AFs, with a mean age of 70.30 ± 6.10 years. Intraoperative findings confirmed PTT entrapment in 38 (29.2%) cases. Bimalleolar

and trimalleolar fractures were predominant, accounting for 43.1% and 35.4%, respectively. The mean follow-up time was 16.80 ± 4.30 months. There was no significant difference between the entrapment and non-entrapment groups. As to baseline characteristics, age, sex, body mass index (BMI), injury side, and fracture type showed no statistically significant differences between the two groups ($p > 0.05$). The incidence rate of osteoporosis in the entrapment group was significantly higher than in the non-entrapment group ($p < 0.05$). In addition, the proportion of patients with posterior AFs and those with a fracture line extending into the PTT sheath on preoperative CT was significantly higher in the entrapment group ($p < 0.05$). A representative preoperative axial CT image demonstrating PTT involvement is shown in Figure 1. The fracture fragment extended into the retromalleolar groove and altered the normal anatomical course of the PTT, resulting in direct compression and potential entrapment. Except for the above factors, there was no statistically significant difference between the two groups in the other baseline clinical characteristics (Table 1).

Intraoperative morphological characteristics of posterior tibial tendon entrapment

A total of 38 patients with intraoperatively confirmed PTT entrapment were documented. Entrapment occurred most frequently in posterior AFs [26 (68.4%)], followed by the medial malleolus fragment [12 (31.6%)]. No PTT entrapment anterior to the tibiotalar joint or at the level of the talonavicular joint was observed.

Nineteen (50.0%) cases showed simple mechanical incarceration of the tendon, with complete continuity of the tendon and no obvious abnormality of the surrounding soft tissue. Fourteen (36.8%) patients exhibited varying degrees of concurrent soft tissue adhesions, presenting as limited tendon mobility while maintaining structural integrity. Additionally, 5 (13.1%) cases had concurrent fiber abrasion or focal injury on the tendon surface during release, but no complete rupture was found. All cases of PTT entrapment were treated intraoperatively, and there was no failure of fracture reduction or need to terminate surgery due to PTT entrapment.

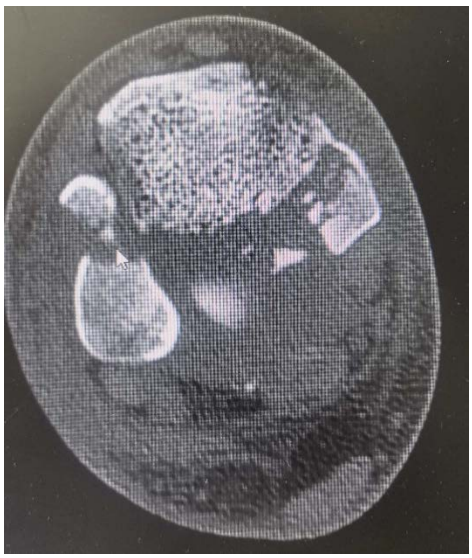

Fig. 1 – Representative preoperative axial computed tomography image demonstrating posterior tibial tendon involvement (arrow).

Table 1

Baseline data

Variable	Group		t/χ^2	*p*-value
	entrapment (n = 38)	non-entrapment (n = 92)		
Age, years	71.34 ± 6.25	69.87 ± 5.93	1.265	0.208
Female	24 (63.1)	54 (58.7)	0.223	0.637
BMI, kg/m²	24.18 ± 2.87	23.62 ± 2.54	1.100	0.273
Left-sided injury	20 (52.6)	46 (50.0)	0.075	0.785
Fractures				
isolated malleolar	6 (15.8)	22 (23.9)	1.050	0.305
bimalleolar	16 (42.1)	40 (43.5)	0.021	0.886
trimalleolar	16 (42.1)	30 (32.6)	1.061	0.303
Osteoporosis	21 (55.3)	30 (32.6)	5.789	0.016
Posterior ankle fracture	30 (79.0)	39 (42.4)	14.430	< 0.001
Fracture line extending into tendon sheath	23 (60.5)	24 (26.1)	13.818	< 0.001
Follow-up duration, months	16.95 ± 4.56	16.78 ± 4.23	0.204	0.839

BMI – body mass index; n – number.

Values are given as numbers (percentages) or mean ± standard deviation.

Predictive results for posterior tibial tendon entrapment using a basic logistic regression model without incorporating imaging enhancement features

The ROC curve analysis showed that the basic LR model without imaging enhancement features achieved an AUC of 0.72, suggesting that the model has moderate and relatively robust discriminatory power (Figure 2). In the model coefficient analysis, posterior AF involvement was the main predictor of PTT entrapment, with a standardized regression coefficient of 1.56 and a corresponding OR of 4.78, suggesting that patients with posterior AFs have a significantly elevated risk of tendon entrapment. Age (OR = 0.57) and osteoporosis (OR = 0.69) were included as adjustment variables in the model, and their effects were attenuated after controlling for fracture morphology.

Comparison of the imaging-enhanced logistic regression model with machine learning models for performance in predicting posterior tibial tendon entrapment

The ROC curve analysis revealed that the discriminatory power of the imaging-enhanced LR model was significantly improved compared with the basic model, achieving an AUC of 0.89, significantly higher than that of the LR model without imaging enhancement features (AUC = 0.72). The RF and SVM models also showed high discriminatory power with AUCs of 0.85 and 0.88, respectively (Figure 3). The classification performance of each model was further evaluated at a fixed predicted probability threshold of 0.5. The results showed that the imaging-enhanced LR model showed a balanced performance between sensitivity (71.1%) and specificity (94.6%), with an overall accuracy of 87.7%. The RF model had relatively high sensitivity (78.9%), but its overall discriminatory power and robustness did not significantly outperform the imaging-enhanced LR model. Although the SVM model achieved the highest specificity (100%) and accuracy (91.5%), its sensitivity did not improve further, and the classification results showed a more extreme distribution pattern. Considering the discriminatory power, classification performance, and model interpretability, the imaging-enhanced LR model demonstrated better robustness and clinical interpretability while maintaining higher predictive performance. Therefore, this model was selected as the primary predictive model for subsequent risk stratification, interpretability analysis, and clinical decision-making processes.

Calibration performance of the imaging-enhanced logistic regression model for predicting posterior tibial tendon entrapment

The calibration curve demonstrated good agreement between the predicted risk and the observed incidence of PTT entrapment across most probability intervals (Figure 4). Although the model's predicted probability was slightly lower than the observed incidence rate in the low-risk interval, the overall trend was generally consistent with the ideal calibration line, with no significant systematic overestimation or underestimation observed. The Brier score was 0.097, indicating acceptable model accuracy and robustness at the predicted probability level. These results indicate that the imaging-enhanced LR model not only possesses good discriminatory power but also has reliable risk estimation performance, providing a basis for subsequent risk stratification and clinical decision-making.

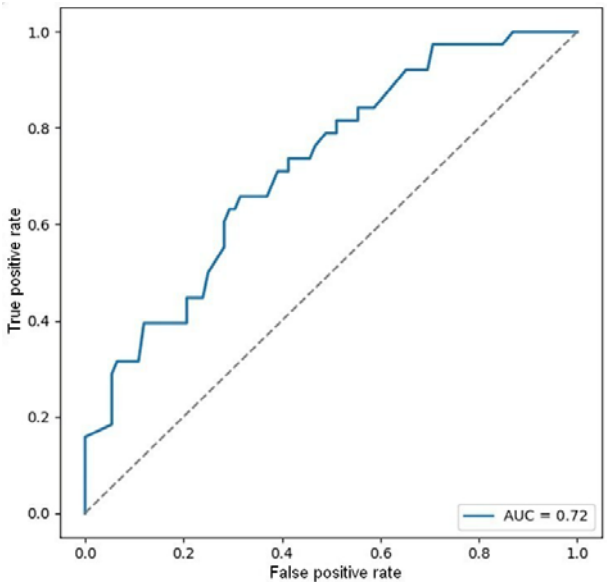

Fig. 2 – Receiver operating characteristic curve for basic clinical logistic regression model without incorporating imaging enhancement features. Dashed lines represent reference lines for random classification. AUC – area under the curve.

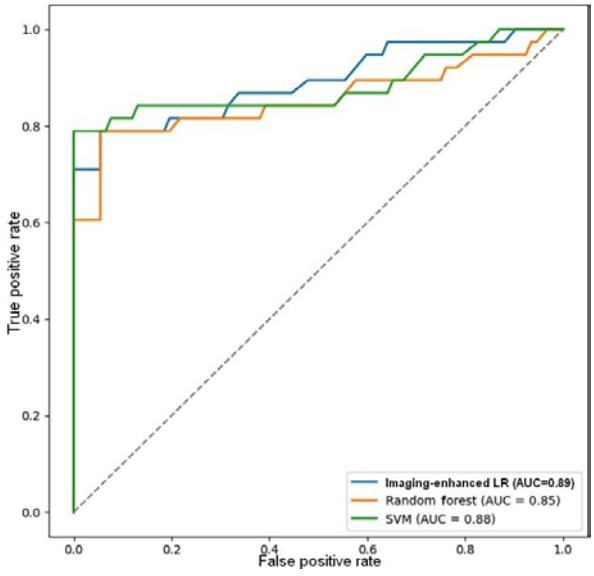

Fig. 3 – Comparison of receiver operating characteristic curves for different predictive models. Dashed lines represent reference lines for random classification. LR – logistic regression; AUC – area under the curve; SVM – support vector machine.

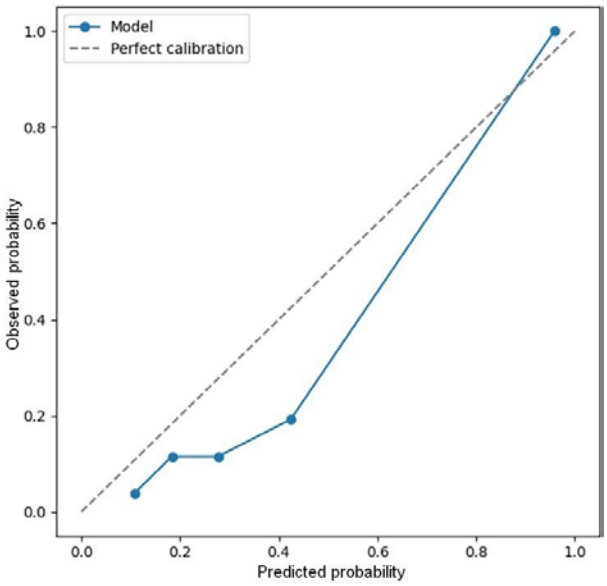

Fig. 4 – Calibration curve of the imaging-enhanced logistic regression model. The dashed line represents the ideal calibration line.

Decision curve analysis of the imaging-enhanced logistic regression model for predicting posterior tibial tendon entrapment

To assess the potential clinical decision-making value of the imaging-enhanced LR model, DCA was further employed to compare its net benefit against "treat-all" and "treat-none" strategies at different threshold probabilities (Figure 5). The results showed that the net benefit of the imaging-enhanced LR model was consistently higher than that of the treat-all and treat-none strategies within the clinically relevant interval of threshold probability of about 0.10–0.50, with a generally stable curve profile. In contrast, the net benefit of the treat-all strategy decreased rapidly as the threshold probability increased, while the treat-none strategy yielded a constant net benefit of zero across all threshold intervals. These findings suggest that, within a reasonable preoperative risk threshold range, preoperative risk assessment and intraoperative exploration decisions based on the imaging-enhanced LR model offer a higher potential net clinical benefit than empirical exploration or no exploration in all patients.

Interpretability analysis of the imaging-enhanced logistic regression model for predicting posterior tibial tendon entrapment

To further elucidate the predictive basis of the imaging-enhanced LR model, the standardized regression coefficients and corresponding ORs of variables in the model were analyzed (Figure 6). The results revealed that imaging structural features dominated the model predictions. CT showed that PTT sheath involvement contributed most significantly to predicting PTT entrapment, with a standardized regression coefficient of 1.98 and an OR of 7.22, suggesting that the risk of tendon entrapment increases significantly when the fracture line extends into the PTT sheath. Posterior AF involvement and more fracture fragments were also significant positive predictors, with a regression coefficient of 0.92 and an OR of 2.52, indicating that fracture complexity and posterior ankle anatomical changes are closely related to tendon entrapment risk. In contrast, age (OR = 0.30) and osteoporosis status (OR = 0.56) exhibited negative or weaker predictive effects in the model, primarily serving as adjustment variables to control for baseline individual differences. Their contribution to the overall predictive power of the model was relatively limited. These results indicate that the predictive performance of the imaging-enhanced LR model primarily derives from anatomical and structural features captured by preoperative imaging, rather than relying solely on individual demographic factors, thereby enhancing the model's interpretability and reliability in clinical application.

Risk stratification analysis of posterior tibial tendon entrapment based on the imaging-enhanced logistic regression model

The actual incidence rate of PTT entrapment showed a clear stepwise distribution across risk groups (Figure 7). In the low-risk group, 49 patients were included, of whom 4 developed PTT entrapment, yielding an incidence rate of 8.2%. The medium-risk group also included 49 patients, 7 (14.3%) of whom had entrapment. In contrast, 32 patients were included in the high-risk group, of whom 27 had intraoperatively confirmed PTT entrapment, with an incidence rate of 84.4%. The incidence rate of PTT entrapment increased significantly with the increase of risk stratification level, suggesting that the model possesses good discriminatory power at the risk stratification level. The above results demonstrate that the imaging-enhanced LR model can not only effectively distinguish patients with different risk levels but also clearly identify high-risk groups, providing a basis for formulating preoperative targeted intraoperative exploration and management strategies.

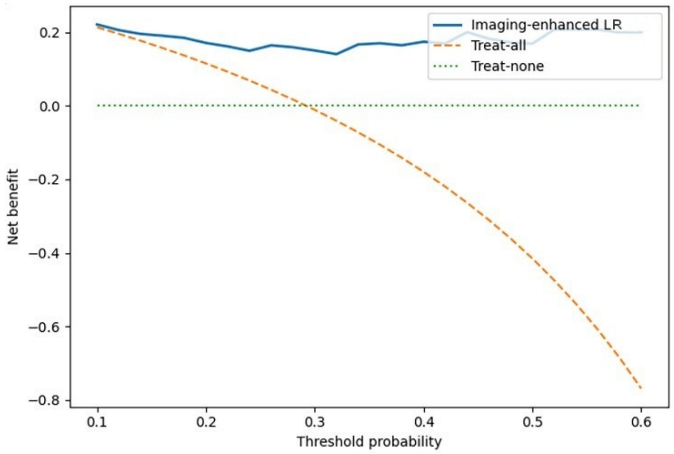

Fig. 5 – Decision curve analysis of the imaging-enhanced logistic regression (LR) model. The net benefit of the imaging-enhanced LR model (solid line) at different threshold probabilities is shown and compared with treat-all (dashed line) and treat-none (dotted line) strategies.

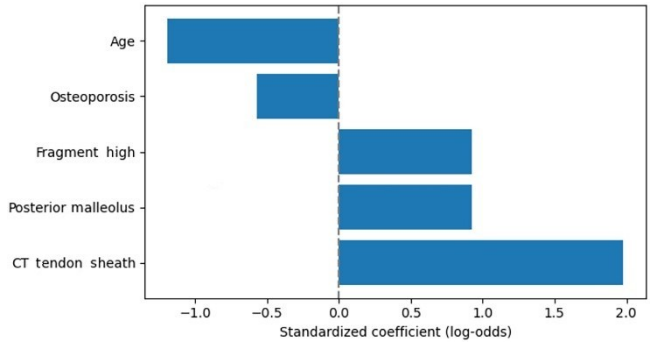

Fig. 6 – Standardized regression coefficients for variables in the imaging-enhanced logistic regression model. The bar chart displays standardized regression coefficients (log-odds) for predictor variables in the model, with positive values indicating an increased risk and negative values indicating a decreased risk. CT – computed tomography.

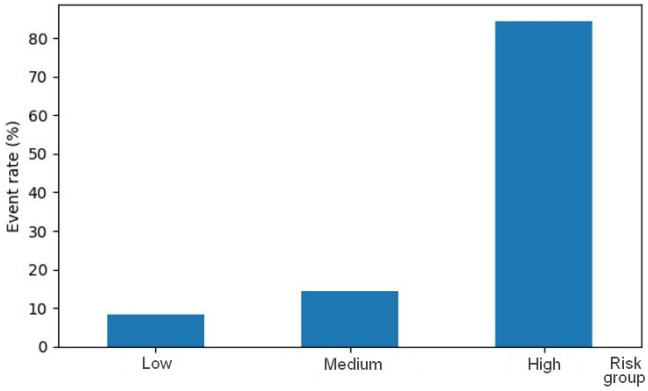

Fig. 7 – Actual incidence rate of posterior tibial tendon entrapment across different risk stratification levels.

Intraoperative grading processing results of posterior tibial tendon entrapment based on preoperative risk stratification

Further analysis of the correlation between preoperative risk stratification and intraoperative entrapment grading showed that patients predicted as low risk preoperatively were more likely to correspond to grades 0–1, and they underwent relatively simple intraoperative management. Medium-risk patients were mainly concentrated in grades 1–2. The proportion of grades 2–3 entrapment was significantly higher in high-risk patients. This denotes that as the preoperative pre-

dicted risk rises, both the intraoperative entrapment grade and the complexity of the procedure correspondingly increase.

Discussion

This study developed and validated an imaging-enhanced predictive model based on preoperative available clinical and imaging data of elderly patients with AFs, enabling preoperative identification of high-risk individuals for PTT entrapment. The results showed that PTT entrapment occurred with a certain frequency (29.2%) in the elderly with AFs, and it was closely associated with the fracture morphology and local anatomical structure changes reflected by preoperative CT. Incorporating imaging structural features significantly enhanced the predictive model's discriminatory power, enabling effective preoperative risk stratification. This provides a reference for determining whether targeted exploration and corresponding management should be performed intraoperatively.

In this study, 29.2% of the elderly patients with AFs were confirmed to have PTT entrapment intraoperatively, indicating a relatively high incidence rate of this complication in this population. The previous report on PTT entrapment has primarily focused on case reports or small-sample retrospective analyses, often treating it as an incidental intraoperative problem, lacking a systematic understanding of its occurrence characteristics [16]. The results of this study suggested that PTT entrapment was common in elderly patients with AFs and that relying solely on routine intraoperative experience may carry a risk of missed diagnosis. Considering the important role of PTT in maintaining medial stability of the ankle joint and arch function, failure to promptly identify and address its intraoperative entrapment may increase surgical complexity and adversely affect postoperative functional recovery [17]. Therefore, systematic evaluation of PTT entrapment holds definite clinical significance in the diagnosis and treatment of AFs in the elderly.

This study revealed that PTT entrapment primarily results from local anatomical changes caused by fractures, a process that can be clearly visualized on preoperative CT imaging. Under normal conditions, PTT runs along the posterior margin of the tibia and behind the medial ankle. Its smooth sliding depends on continuous bony structures and a relatively intact tendon sheath environment [18, 19]. When AFs involve the posterior ankle, especially comminuted fractures, the integrity of the posterior tibial margin is disrupted, and the originally smooth sliding interface is replaced by irregular fracture sections or loose bone fragments [20]. During fracture reduction and internal fixation, these changes create potential mechanical entrapment points along the tendon course. If the fracture line further involves the PTT sheath, the surrounding tendon sheath structures and soft tissue barriers become compromised, significantly increasing the likelihood of direct contact between the tendon and fracture fragments [21]. In such cases, even if the overall reduction of the fracture proceeds smoothly, PTT may still be passively embedded in the fracture gap due to local space constraints, resulting in entrapment that is difficult to detect immediately intraoperatively [22]. At the same time, a comminuted fracture is often accompanied by extensive local soft tissue injury and disrupted anatomical relationships. This complex fracture morphology not only increases the probability of PTT entrapment, but also creates conditions for the subsequent formation of soft tissue adhesion [23]. In this study, the intraoperative morphological observation aligned with these hypotheses. Among patients with PTT entrapment, entrapment predominantly occurred within the posterior AF gap, and only about half of the cases showed simple mechanical incarceration. A considerable number of patients had concurrent soft tissue adhesion of varying degrees, and a few cases even had concurrent tendon surface injury. In contrast, demographic factors such as age and sex had relatively limited predictive value in the model and did not directly contribute to the formation of PTT entrapment. Based on the above findings, it can be concluded that the occurrence of PTT entrapment is mainly related to the change in fracture morphology and local anatomical relationship, and its risk mainly depends on the relationship between bone and soft tissue shown by preoperative imaging, which mechanistically supports the rationale for systematic assessment using preoperative CT scans.

Based on the close relationships of PTT entrapment with fracture morphology and local anatomical changes, this study incorporated relevant imaging features into the predictive model and further evaluated their value in preoperative risk identification and clinical decision-making. The results showed that incorporating imaging data such as the number of fracture fragments and PTT sheath involvement significantly enhanced the model's discriminatory and risk stratification capabilities (AUC 0.72 vs. 0.89). This improvement was reflected not only in the enhancement of overall discriminatory power but also in the identification of high-risk patients. Following risk stratification based on the model's predicted probabilities, the actual incidence of PTT entrapment demonstrated a distinct gradient across risk tiers, with the high-risk group exhibiting a significantly higher rate of intraoperatively confirmed entrapment. The results suggest that the imaging-enhanced model not only statistically improves predictive performance but also distinguishes patients with a genuine risk of PTT entrapment preoperatively, making the predictive results closer to the real surgical scenarios. Furthermore, DCA showed that preoperative assessment based on the imaging-enhanced model resulted in higher net benefit and better decision performance than routine exploration or no exploration for all patients within clinically common threshold probabilities. These findings demonstrate that incorporating imaging structural features not only significantly enhances the discriminatory power of the model but also increases its practical value in preoperative risk stratification and intraoperative decision support.

Some limitations are worth noting in this study. Firstly, as a single-center retrospective study with a relatively

limited sample size, further validation of the model's robustness and external applicability through multicenter studies is required. Secondly, intraoperative morphologic assessment and management strategies depend to some extent on surgeon experience, potentially introducing observer variability. Future studies incorporating a prospective design can be conducted to validate the imaging predictive results across different surgeons and clinical settings, thereby further improving the preoperative assessment and intraoperative management process of PTT entrapment.

Conclusion

In conclusion, posterior tibial tendon entrapment occurs with a certain frequency in elderly patients with ankle fractures, warranting clear clinical attention. Based on fracture morphology and local anatomical structure reflected by preoperative computed tomography, a relatively reliable preoperative assessment of posterior tibial tendon entrapment risk can be performed. Compared with prediction methods that rely solely on basic clinical characteristics, predictive models incorporating imaging features significantly improve risk identification and effectively stratify high-risk patients preoperatively. Combined with intraoperative morphological validation results, the imaging-enhanced model has potential clinical value in guiding preoperative evaluation and optimizing intraoperative management strategies.

Conflict of interest

The authors declare no conflict of interest.

R E F E R E N C E S

1. *Ayala-Ortiz JL, Alcaide DM, Taylor S, McGwin G, Johnson JP.* Trends in geriatric ankle fractures in the United States: An 8-year analysis. Injury 2026; 57(3): 113066. DOI: 10.1016/j.injury.2026.113066.
2. *Mason L, Orji C, Szatkowski J.* Management of Geriatric Ankle Fractures. Curr Osteoporos Rep 2025; 23(1): 48. DOI: 10.1007/s11914-025-00940-3.
3. *Raschke MJ, Ochman S, Milstrey A.* Ankle fractures in the elderly: Do we have new concepts? EFORT Open Rev 2023; 8(5): 223–30. DOI: 10.1530/EOR-23-0052.
4. *Egu C, Akil H, Hakim RA, Badhe N, Essiet E, Akintunde S,* et al. Early vs Late Weight Bearing After Ankle Fracture Fixation: A Meta-analysis of Randomized Controlled Trials. Foot Ankle Int 2025; 47(2): 174–83. DOI: 10.1177/10711007251392223.
5. *Mair O, Pflüger P, Hanschen M, Biberthaler P, Crönlein M.* Treatment strategies for complex ankle fractures-current developments summarized in a narrative review. Ann Transl Med 2023; 11(11): 387. DOI: 10.21037/atm-23-1173.
6. *Wang J, Latt LD, Martin RD, Mannen EM.* Postural Control Differences between Patients with Posterior Tibial Tendon Dysfunction and Healthy People during Gait. Int J Environ Res Public Health 2022; 19(3): 1301. DOI: 10.3390/ijerph19031301.
7. *Aamir J, Syziu A, Andritsos L, Caldwell R, Mason L.* Tibialis posterior tendon entrapment in posterior malleolar and pilon injuries of the ankle: a retrospective analysis. Eur J Orthop Surg Traumatol 2024; 34(2): 781–7. DOI: 10.1007/s00590-023-03714-8.
8. *Nguyen Van L, Nguyen Nang G.* Ankle fracture-dislocation with the interposition of the tibialis posterior tendon in the ankle syndesmosis and tibiotalar joint - A case report and systematic literature review. Int J Surg Case Rep 2023; 110: 108710. DOI: 10.1016/j.ijscr.2023.108710.
9. *Nohmi S, Ogawa T.* Delayed diagnosis of posterior tibialis tendon interposition in the distal tibiofibular and tibiotalar joints after open fracture-dislocation of the ankle joint: A case report with a 10-year follow-up. Trauma Case Rep 2025; 55: 101134. DOI: 10.1016/j.tcr.2025.101134.
10. *Syziu A, Aamir J, Mason LW.* Posterior tibialis tendon entrapment as a complication of posterior malleolar fractures in complex ankle fractures. Bone Jt Open 2024; 5(3): 252–9. DOI: 10.1302/2633-1462.53.BJO-2023-0139.
11. *Colomb E, Muscatelli S, Morash JG, Crawford EA, Holmes JR, Walton DM.* Irreducible fractures and dislocations of the ankle associated with entrapment of the posterior tibial tendon within the tibiofibular interosseous space: a case series and literature review. Foot Ankle Orthop 2021; 6(2): 24730114211000297. DOI: 10.1177/24730114211000297.
12. *Ziegler P, Bahrs C, Konrads C, Hemmann P, Ahrend MD.* Ankle fractures of the geriatric patient: a narrative review. EFORT Open Rev 2023; 8(1): 1–10. DOI: 10.1530/EOR-22-0082.
13. *Han H, Choi JH, Lee KM.* Interposition of posterior tibial tendon in tibiofibular syndesmosis in a bimalleolar ankle fracture: a case report. Acta Orthop Traumatol Turc 2022; 56(6): 412–5. D: 10.5152/j.aott.2022.22098.
14. *LeBoff MS, Greenspan SL, Insogna KL, Lewiecki EM, Saag KG, Singer AJ,* et al. The clinician's guide to prevention and treatment of osteoporosis. Osteoporos Int 2022; 33(10): 2049–102. DOI: 10.1007/s00198-021-05900-y. Erratum in: Osteoporos Int 2022; 33(10): 2243. DOI: 10.1007/s00198-022-06479-8.
15. *Terstegen J, Weel H, Frosch KH, Rolvien T, Schlickewei C, Mueller E.* Classifications of posterior malleolar fractures: a systematic literature review. Arch Orthop Trauma Surg 2023; 143(7): 4181–220. DOI: 10.1007/s00402-022-04643-7.
16. *Amaro P, Ferreira J, Viegas R, Protásio J, Vide J, Mendes D.* Posterior tibial tendon entrapment after fracture dislocation of the ankle. Foot Ankle Surg Tech Rep Cases 2022; 2(1): 100125. DOI: 10.1016/j.fastrc.2021.100125.
17. *Ptak NA, Rigby RB.* Subluxation of the posterior tibial tendon into the tibiofibular syndesmosis secondary to high-level ankle fracture or dislocation: Surgical reduction technique guide and case study. Foot Ankle Surg 2024; 4(1): 100357. DOI: 10.1016/j.fastrc.2023.100357.
18. *Oddy MJ, Choraria A, Campbell A, Ali A, Rajesparan K.* Tibial Retro-Malleolar Groove Morphology in Patients With Posterior Tibialis Tendon Dysfunction. J Foot Ankle Surg 2023; 62(5): 888–92. DOI: 10.1053/j.jfas.2023.06.003.
19. *González-Gutiérrez O, Roldan-Valadez E, Molina-Gonzalez M, Garcia-de-Bustamante MR, López-Montoya LO, Gonzalez-Trejo AP,* et al. Imaging Anatomy of the Ankle in Normal and Pathological States: A Clinically Focused Pictorial Review. Cureus 2025; 17(10): e93882. DOI: 10.7759/cureus.93882.
20. *Ribeiro HC, Mayer WP, Matz J, Baptista JDS.* Posterior Malleolus: Morphologic Classification, Morphometry, and Clinical Insights. Foot Ankle Orthop 2025; 10(2): 24730114251341900. DOI: 10.1177/24730114251341900.
21. *Thomas S, Huang BK, Korrapati A, O'Leary B, Gurusamy P, O'Leary R,* et al. The effect of spanning external fixation on en-

trapped structures in tibial pilon fractures. Eur J Orthop Surg Traumatol 2024; 34(1): 237–42. DOI: 10.1007/s00590-023-03641-8.

22. *Chidda A, Kim J, Golub I, Chien BY, Kwon JY*. Intra-articular Posterior Tibial Tendon Entrapment in an Ankle Fracture Mimicking Syndesmotic Malreduction: A Case Report. Foot Ankle Orthop 2025; 10(4): 24730114251386023. DOI: 10.1177/24730114251386023.

23. *Mombello F, Vera G, Rammelt S*. Pilon Fractures: Update on treatment. J Foot Ankle 2024; 18(3): 274–91. DOI: 10.30795/jfootankle.2024.v18.1857.5.

Received on March 5, 2026
Revised on April 5, 2026
Revised on April 19, 2026
Accepted on April 29, 2026
Online First June 2026